# TES-PS10 Postmortem tests: Carbon steel corrosion performance exposed to molten salts under relevant operation conditions and lessons learnt for commercial scale-up

F. Javier Ruiz-Cabañas[1,*], Cristina Prieto[1,2], Virginia Madina[3], A. Inés Fernández[4], Luisa F. Cabeza[5]

[1]Abengoa Energía, Solar Technology department, Energía Solar 1, 41014, Sevilla, Spain

[2] Department of Energy Engineering, Universidad de Sevilla, Camino de los Descubrimiento s/n, 41092, Spain

[3] Materials and Processes Area. Tecnalia Research and Innovation, Mikeletegi Pasealekua, 2, 20009 San Sebastián, Spain

[4]Department of Materials Science & Physical Chemistry, Universitat de Barcelona, Martí i Franqués 1-11, 08028 Barcelona, Spain

[5]GREiA Research Group, INSPIRES Research Centre, Universitat de Lleida, Pere de Cabrera s/n, Lleida, Spain

* Corresponding author: F. Javier Ruiz-Cabañas

## Abstract

Postmortem tests were performed over components removed from the TES-PS10 pilot plant after almost four years of continuous operation being exposed to solar salts under representative commercial operation conditions. Accordingly, corrosion performance of plates sections extracted from both storage tanks and samples cut from the hot molten salts pump were evaluated. Corrosion damage extension, oxides layers morphology, and corrosion products chemistry were analyzed by X-Ray diffraction, energy dispersive X-ray spectrometry, optical microscopy, and SEM. In addition to materials compatibility with molten salts, mechanical tests were carried out over the storage tanks plates sections. Although the corrosion damage extension over the plates extracted from storage tanks was low and the mechanical properties were according to the standard, some interesting observations were seen. For example, a sample extracted from the hot storage tank and exposed to intermittent contact with molten salts showed some areas characterized by the growth of a non-protective oxide scale. Moreover, localized corrosion with slight penetration through the base material was identified for all storage plates samples under evaluation. On the other hand, the molten salt pump parts under study showed adherent and uniform oxides layers without detecting corrosion-erosion phenomena. Some cavities were found in the discharge elbow, and these imperfections were associated to a bad metallurgical quality during casting. Summarizing, corrosion phenomena suffered by the components under evaluation could be corrected in future plants by applying the lessons learned discussed in this study. As conclusion, materials selection analyzed within this postmortem evaluation is valid from the corrosion point of view to be used in the design of commercial TES systems in PTC plants.

*Keywords: Postmortem; Corrosion; TES-PS10; Solar salts; Carbon Steel; Lessons Learnt*

## 1. Introduction

Concentrating solar power (CSP) is the technology that uses the energy coming from solar radiation to produce electricity. This process is carried out in power facilities concentrating the direct solar radiation by using mirrored surfaces (concentrator) to increase the temperature of a heat transfer fluid (HTF) which circulates through a receiver. Some technologies use this HTF directly to carry out the thermodynamic conversion cycle in the turbine of the installation to produce electricity. On the other hand, CSP power plants could also use the HTF as an intermediate fluid being necessary a heat exchanger to transfer its energy to the fluid that will be finally used in the turbine [1,2].

The different configurations between concentrator and receiver distinguish the different CSP technologies existing today. Depending on the type of concentrator, these technologies can be classified as follows: (i) parabolic trough collectors [3], (ii) tower [4], (iii) Fresnel collectors [5], and (iv) parabolic dishes [6]. Nowadays, the most mature configuration worldwide is the parabolic trough collectors (PTC) technology using thermal oil as HTF to produce electricity by transferring its thermal energy to steam which is finally pumped to move the turbine of the installation. One of the main advantages of the PTC technology is the possibility of satisfying the daily electricity demand, even considering the fluctuations of the solar resource, by integrating large scale thermal energy storage (TES) systems. Accordingly, TES systems stabilize the production of electricity adapting the installation production to the energy demand and expanding the production with a better efficiency in the solar energy conversion to electricity [7-9]. Nowadays, commercial PTC TES systems use a nitrate salts mixture as storage medium. This inorganic mixture is composed by 60wt.% $NaNO_3$ and 40wt.% $KNO_3$, the so-called solar salts. $NaNO_3$ percentage used is higher than the eutectic composition to obtain a technical-economical optimum. Accordingly, the final price of the mixture decreases due to the associated cost of $NaNO_3$ is lower than $KNO_3$. On the other hand, the molten salt mixture freezing point is penalized, since the eutectic composition one is lower and uses less parasitic electricity. Additional characteristics such as low vapor pressure, high energy density, high thermal stability up to 600 ºC in addition to non-flammable and non-toxic performance make these salts proper candidates for thermal storage fluids to be used in TES systems for PTC power plants [10-13].

Molten salts corrosiveness is one of the most important drawbacks inherent to this fluid at high temperature, being a critical factor to consider for the design of commercial TES systems in PTC facilities. Therefore, the use of inappropriate materials or not considering enough corrosion allowances to withstand a continuous operation in the range of 25-35 years could result in the deterioration of the metal alloys used in the design and construction of such plants, which would mean premature failures due to corrosion, jeopardizing the lifetime of TES system components (storage tanks, piping, molten salts pumps, heat exchanger, valves, instrumentation, among others) and the overall power plant production. The corrosive effect of solar salts is associated to the nitrate-nitrite equilibrium of this mixture at a given temperature. Once the reduction reaction from nitrate to nitrite is produced, the anionic oxidation of the alloy is produced in the corrosive medium via the following reactions (iron is taken as an example) [16-20]. Following reactions show the chemistry involved in the $NaNO_3$-$KNO_3$ system and oxidation process:

$$NO_3^- \leftrightarrow NO_2^- + \frac{1}{2}O_2 \tag{1}$$

$$NO_3^- \rightarrow NO_2^+ + O^{2-} \tag{2}$$

$$NO_2^- \leftrightarrow NO^+ + O^{2-} \tag{3}$$

$$NO_2^- \leftrightarrow NO + O^- \tag{4}$$

$$O^{2-} + NO_3^- \leftrightarrow O_2^{2-} + NO_2^- \tag{5}$$

$$O_2^{2-} + 2NO_3^- \leftrightarrow 2O_2^- + 2NO_2^- \tag{6}$$

$$O^{2-} + \frac{1}{2}O_2 \leftrightarrow O_2^{2-} \tag{7}$$

$$O_2^{2-} + O_2 \leftrightarrow 2O_2^- \tag{8}$$

$$Fe + O^{2-} \leftrightarrow FeO + 2e^- \tag{9}$$

$$3FeO + O^{2-} \leftrightarrow Fe_3O_4 + 2e^- \tag{10}$$

A study of the state-of-the-art shows that the corrosion performance of metal alloys in contact with nitrate salts mixtures at different temperatures was evaluated by different authors. These studies include molten salts compatibility of carbon steels, low and medium alloyed steels, stainless steels, and superalloys proposed for the manufacturing of components used in CSP facilities [21-27]. On the other hand, the effect of impurities in nitrates salts such as chlorides was analyzed in detail showing the importance of controlling the amount in the final mixture to avoid high corrosion damage over metal alloys [28-30]. Nevertheless, most of scientific contributions show results obtained at laboratory scale under controlled conditions and, therefore, a lack of knowledge is detected concerning corrosion performance of metals in contact with solar salt under real operating conditions. Although the materials selection and associated corrosion allowances of commercial TES systems for PTC power plants could be carried out based on these literature data, more representative tests would be desirable for a confident long-term design. Previous studies carried out by the authors of this paper showed the corrosion performance of carbon steel after being exposed to solar salts in a pilot TES system (TES-PS10 plant) during more than 8500 hours under real operation conditions [31]. Therefore, a corrosion testing device (CTD) was designed to evaluate corrosion behavior of materials inside high temperature nitrate salts storage tanks in operation. These results provide a high added value for the design of PTC TES system due to tests boundary conditions in terms of temperature, fluid, and operation strategies are fully aligned with the ones expected in a commercial power plant.

In addition to in-situ corrosion tests under relevant conditions as discussed before, postmortem evaluations become an interesting analysis to determine the status of materials after the shut-down of a facility once the life time of the plant has expired. Then, postmortem tests are a powerful tool to validate the mechanical design of the installation providing the following information: (i) to analyze the corrosion performance of materials selection under real operation, (ii) to identify possible corrosion damages not detectable at laboratory scale due to difficulties to reproduce commercial operation conditions, and (iii) to obtain feedback about materials selection and design guidelines to be used in commercial projects.

The research within this paper is based on components postmortem analysis carried out in the TES-PS10 pilot plant facility built by Abengoa to test the PTC TES systems prior to the design of commercial projects with this technology [32,33]. The postmortem tests were performed after more than 30000 hours of operation under representative commercial operation conditions. Storage fluid analysis is not within the scope of this study, which is focused on the corrosion performance of storage tanks and pumping systems. Results provide understanding of corrosion performance of materials typically used for this application and lessons learnt to take into account for TES systems design to be integrated in PTC facilities at commercial scale.

## 2. Materials and methods

### 2.1. TES-PS10 pilot plant

Postmortem analyses were performed over components extracted from the TES-PS10 pilot plant (Figure 1). The TES-PS10 test facility was an indirect double tank storage system with a thermal capacity of 8.1 $MWh_{th}$ and 450 Ton of molten salts inventory (Figure 1b). This pilot plant was coupled to another demo installation called Repow, consisting of a 600 meter-long parabolic trough solar field using thermal oil as heat transfer fluid (eutectic mixture of biphenyl and diphenyl oxide). TES-PS10 pilot plant was designed and built in 2008 starting operation in January 2009, being the first worldwide experience of a CSP oil trough pilot plant with molten salts storage achieving a technology readiness level TRL-9 (Figure 1a). Daily operation for both plants was focused in the following two operations modes up to December 2012 when the shut-down of the installation was executed: (i) during the charge mode, hot HTF from the solar field was pumped to TES system heat exchanger and molten salts stored in the cold tank were also pumped to this equipment. Thermal transference between HTF and molten salts was executed in the heat exchanger. Then, molten salts were heated and stored in the hot tank of TES-PS10 facility; (ii) during discharge mode, molten salts stored in the hot tank and cold HTF were pumped through the heat exchanger. Molten salts were cooled and stored in the cold tank and hot HTF was pumped to the steam generation area. While the hot tank molten salt temperature was 390 ºC, cold tank temperature was fixed at 290 ºC using nitrogen as cover gas for both vessels. The storage fluid used in the TES-PS10 was the so-called solar salt, 60wt.% $NaNO_3$ and 40wt.% $KNO_3$. $NaNO_3$ industrial grade and $KNO_3$ technical grade were provided by SQM and Haldor Topsoe, respectively. Their purity and main impurities breakdown are specified in Table 1.

**Table 1. Purity and impurities for $NaNO_3$ and $KNO_3$ salts used as storage fluid in TES-PS10 pilot plant**

| Purity/Impurities | $NaNO_3$ | $KNO_3$ |
|---|---|---|
| **Purity (wt.%)** | 98 min | 98 min |
| **Chloride (wt.%)** | 0.6 max | 0.015 max |
| **Sulfate (wt.%)** | 0.50 max | 0.05 max |
| **Carbonate (wt.%)** | 0.10 max | Not Specified |
| **Nitrite (wt.%)** | 0.02 max | 0.2 max |
| **Magnesium (wt.%)** | 0.1 max | 0.001 max |

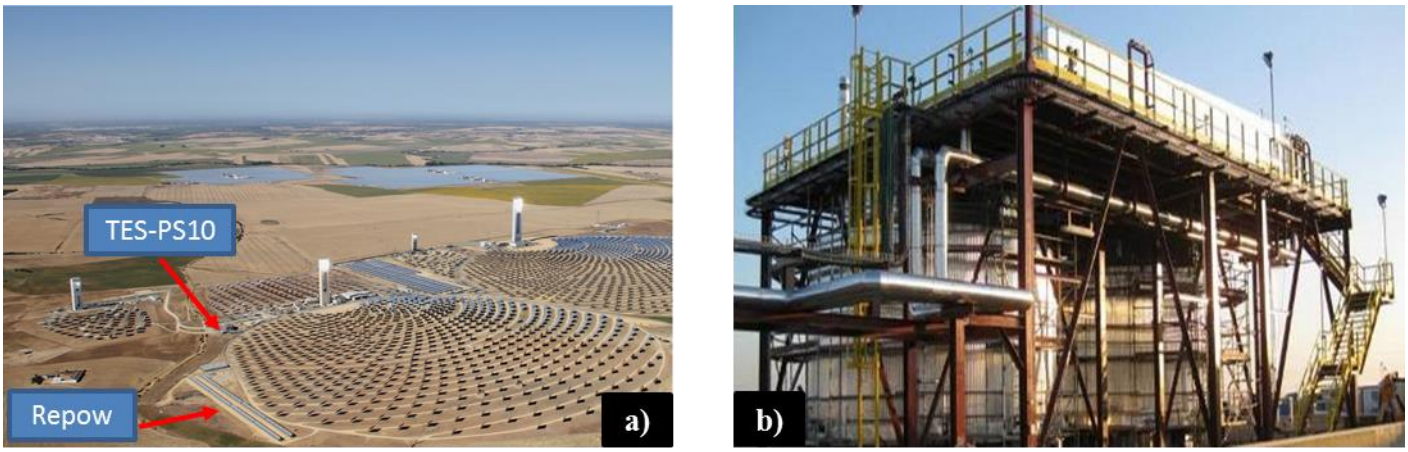


**Figure 1. (a) Solucar Complex overview highlighting TES-PS10 and Repow location; (b) TES-PS10 pilot plant overview**

## 2.2. Components to be evaluated

Several components of the installation were evaluated after the facility shut-down in order to characterize corrosion damage suffered by materials after more than 30000 hours in operation: (i) tank shells and (ii) molten salts pump sections. Two different tank shell sections were extracted from both cold and hot storage vessels. The first section was cut from the upper part of the shell and the other one was extracted from the lower part assuring that all time was submerged in molten salts (Figure 2). Accordingly, the differences between cold and hot temperature exposition were analyzed. Moreover, the corrosion performance of steel depending on molten salts exposure, continuous or intermittent, was also evaluated. Tank shells were manufactured in A516 Gr70 carbon steel. A516 Gr70 is typically used for the manufacturing of pressure vessels and boilers operating in industrial applications at moderate temperatures. On the other hand, hot molten salts pump was removed from the installation to analyze the corrosion performance of two shaft sections through which molten salts flow: discharge elbow and discharge pipe (Figure 3). Therefore, possible corrosion-erosion phenomena produced by molten salts pumping were also evaluated within these components. While the discharge pipe was manufactured in low carbon steel, the discharge elbow was fabricated using ASTM A27 cast carbon steel. Summarizing, six different component sections manufactured in carbon steel were removed for a detailed analysis of materials compatibility after the facility shut-down.

Exposure conditions for the different components under evaluation are are detailed below. Table 2 summarizes exposition and temperature for each component during the operation of the strage system.

- Upper Hot Tank Shell Plate (UHT) and Upper Cold Tank Shell Plate (UCT). Exposed to preheating gases at the beginning of the plant. During operation of the pilot plant (30000 hours), upper plates were exposed to nitrates salts and $N_2$ depending on the level of the salt inventory in the tank.

- Lower Hot Tank Shell Plate (LHT) and Lower Cold Tank Shell Plate (LCT). Exposed to preheating gases at the beginning of the plant. Plates were exposed to nitrates salts during all time due to these sections were located below the minimum salts level of the tank.

Discharge pipe (DP) and Discharge Elbow. Exposed to preheating gases at the beginning of the plant. pumps parts were exposed to nitrates salts during all time due to these pump sections were continuously submerged in molten salts.

**Table 2. Components list extracted from TES-PS10 pilot plant for characterization**

| Component | Exposure | Temperature (ºC) | Reference |
|---|---|---|---|
| Upper Hot Tank Shell Plate | Tank preheating gases<br>Nitrates, $N_2$ | 390 | UHT |
| Lower Hot Tank Shell Plate | Tank preheating gases<br>Nitrates | 390 | LHT |
| Upper Cold Tank Shell Plate | Tank preheating gases<br>Nitrates, $N_2$ | 290 | UCT |
| Lower Cold Tank Shell Plate | Tank preheating gases<br>Nitrates | 290 | LCT |
| Discharge pipe | Tank preheating gases<br>Nitrates | 390 | DP |
| Discharge Elbow | Tank preheating gases<br>Nitrates | 390 | DE |

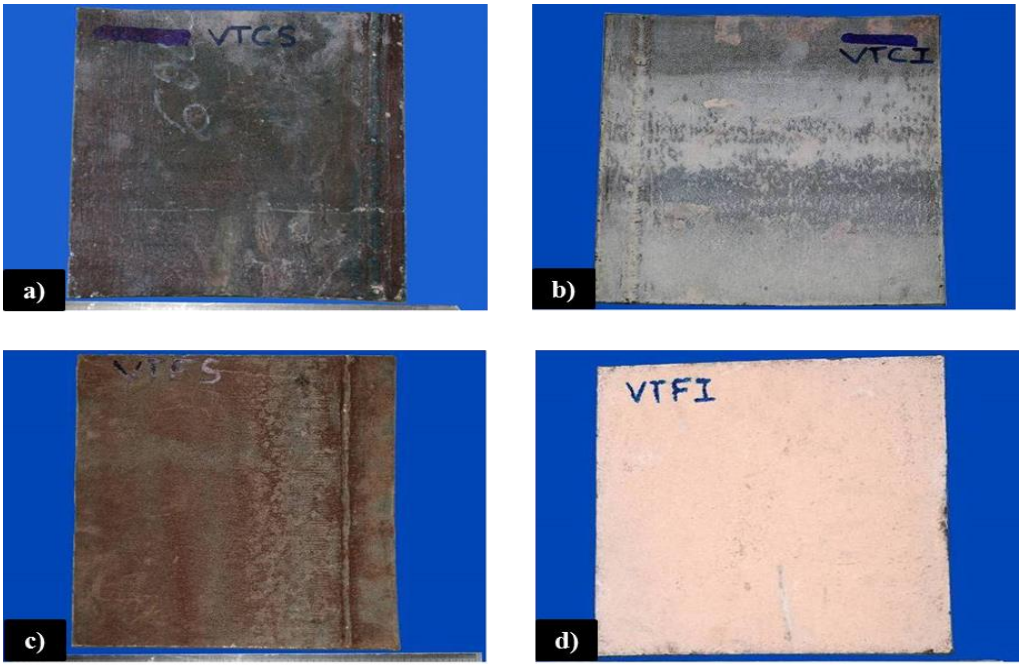


**Figure 2. Storage tanks shell sections. (a) upper hot tank (UHT) shell plate section; (b) lower hot tank (LHT) shell plate section; (c) upper cold tank (UCT) shell plate section; (d) lower cold tank (LCT) shell plate section**

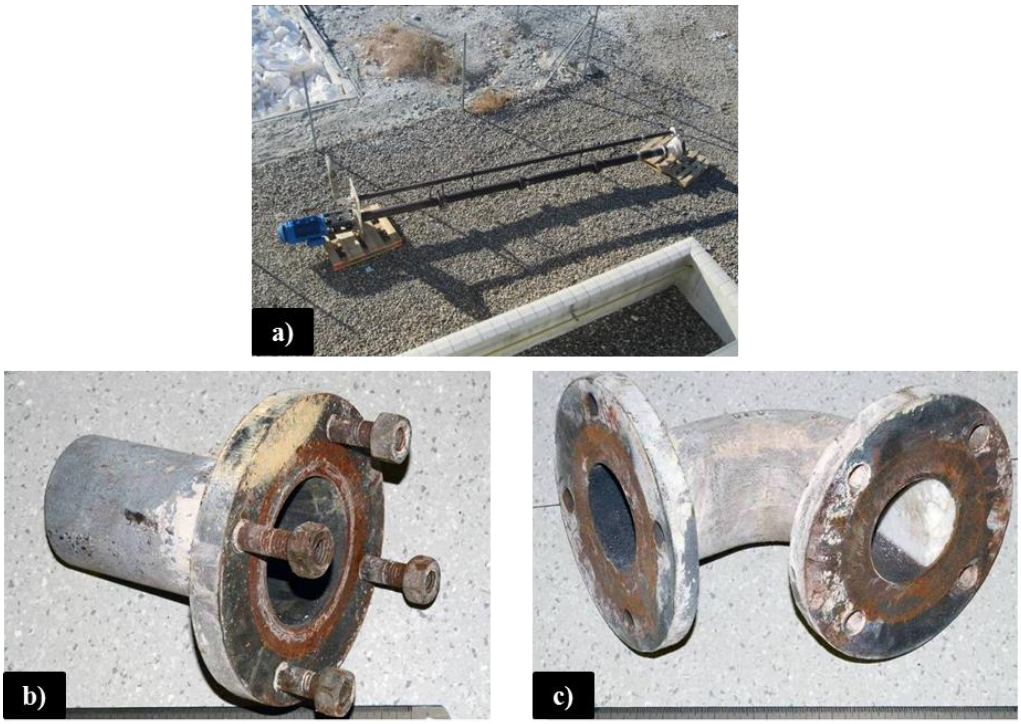


**Figure 3. Hot molten salts pump. (a) Molten salts pump removed from the hot storage tank; (b) Discharge pipe section; (c) Discharge elbow section**

## 2.3. Methodology

After the facility shut-down, components sections exposed in Table 2 were extracted from the TES-PS10 pilot plant to analyze the corrosion performance of each one. All components were preliminary evaluated by visual inspection to have an overall overview of the status of the material after almost four years of operation in the facility. Accordingly, samples were cut for a deep visual analysis of both, internal and external surfaces. Metallographic specimens were extracted to analyze the corrosion products generated over the base metal by surface microscopy using an electron scanning microscope (SEM-JEOL 5910-LV). In addition to oxides layer morphology, chemical composition of the corrosion products was evaluated by energy dispersive spectroscopy (EDS) spectra. A microanalyzer (EDSOXFORD INCAx-act) coupled to a SEM was used to characterize the different alloying elements involved in the oxides layers developed by the different components under evaluation (detection limit of EDS technique is around 1000 ppm). On the other hand, X-Ray diffraction (XRD) was used to identify oxides stoichiometry (Bruker D8 Advance XRD). Microstructural characterization was performed over transversal metallographic specimens to analyze the corrosion morphology through the cross-section and corrosion damage penetration by means of an optical microscopy. Localized phenomena such as oxides layers delamination/exfoliation, pitting or other specific attack suffered by carbon steels samples would be confirmed within this characterization stage. In addition to corrosion attack progression, corrosion products morphology and oxides layers chemical evaluation, mechanical characterization of tank shells sections was performed. Accordingly, tensile tests were executed over tensile specimens cut from the different plates to obtain values associated to yield strength, tensile strength and elongation. Tensile tests were performed at room temperature in accordance with ASTM E8-2011 Standard. Results were compared with the reference ones extracted from the standard to identify if long-term exposition to high temperature molten salts produced any

drastic reduction in the mechanical parameters of the material jeopardizing the structural design of the storage tanks.

## 3. Results and discussion

### 3.1. Tank walls evaluation

**Visual Inspection**

Generalized corrosion was observed on the UHT plate surface generating an irregular reddish-brown oxide layer (Figure 4a). The plate showed areas in which the oxide layer was detached as well as small areas with somewhat larger corrosion product generation. These areas were examined more in detail in the SEM/EDS analysis. On the other hand, the LHT plate showed abundant nitrate salt deposits which were partially cleaned using distilled water for a detailed examination of the metal surface. Then, a generalized corrosion could be observed with the formation of a reddish-brown oxide layer, slightly less thick than the one observed on the UHT sample. Corrosion products were also partially detached in some areas (Figure 4b). The UCT plate, Figure 4b, showed a generalized corrosion on its surface with a formation of an apparently compact reddish-brown oxide layer. Finally, the LCT shell section showed a general and fairly uniform corrosion with a reddish-brown oxide layer formation.

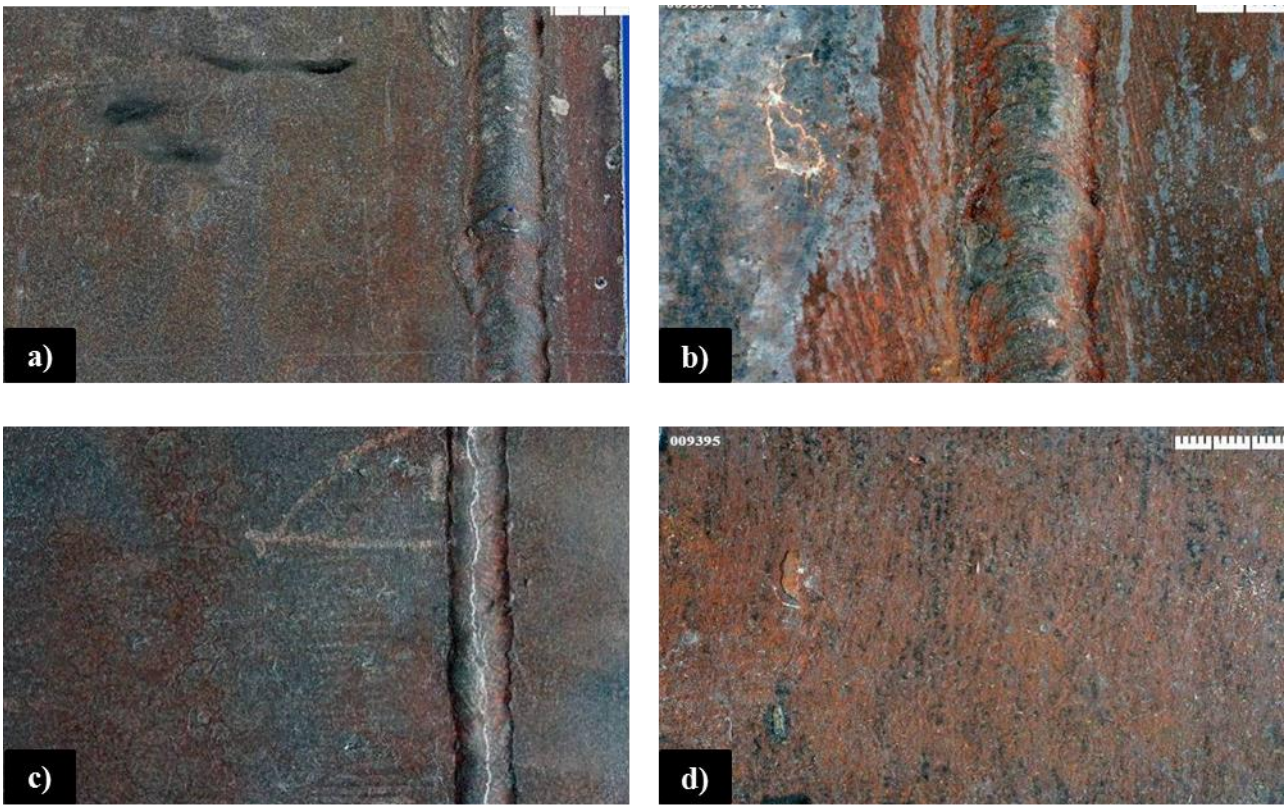


**Figure 4. Storage tanks shell sections visual inspection. (a) upper hot tank (UHT) shell plate section; (b) lower hot tank (LHT) shell plate section; (c) upper cold tank (UCT) shell plate section; (d) lower cold tank (LCT) shell plate section**

**Surface SEM/EDS analysis and XRD**

Figures 5 includes several micrographs of the corrosion products generated on the surface of the UHT plate. The oxide layer had a certain exfoliating and/or laminating nature in some areas (Figure 5a). EDS spectra associated to this layer indicated that it was basically comprised of iron (Fe) and oxygen (O), as iron oxide, together with significant quantities of sodium (Na), potassium (K) and magnesium (Mg) coming from nitrates salts (Figure 5b). Magnesium is typically in the form of magnesium oxide due to the decomposition of magnesium nitrate which is one of the impurities of sodium and potassium nitrates [34]. SEM micrographs clearly showed the generation of more reddish and voluminous corrosion products in specific areas (Figure 5c). EDS spectra over these corrosion nodules showed chloride not previously detected in addition to iron oxide and nitrate salt residue (Figure 5d). The surface analysis of the LHT plate showed a relatively compact and firmly attached oxide layer, with no evidence of exfoliation unlike what was detected in UHT plates (Figure 5e). Small reddish corrosion spots were also detected in some areas of LHT plates corresponding to micro-areas of localized corrosion. Associated EDS spectrum also showed chloride as one of the elements present in the chemical composition of the corrosion nodule (Figure 5f). On the other hand, Figure 6 displayed different views of the oxide layer generated over UCT and LCT tanks shell sections being the corrosion morphology practically identical for both plates. Micrographs highlighted some areas where corrosion products were detached without exfoliation phenomena (Figure 6a). Sections extracted from cold tank also evidenced micro-areas of localized corrosion (Figure 6b and Figure 6c). Finally, UCT and LCT shell EDS spectra were like ones obtained for hot tank.

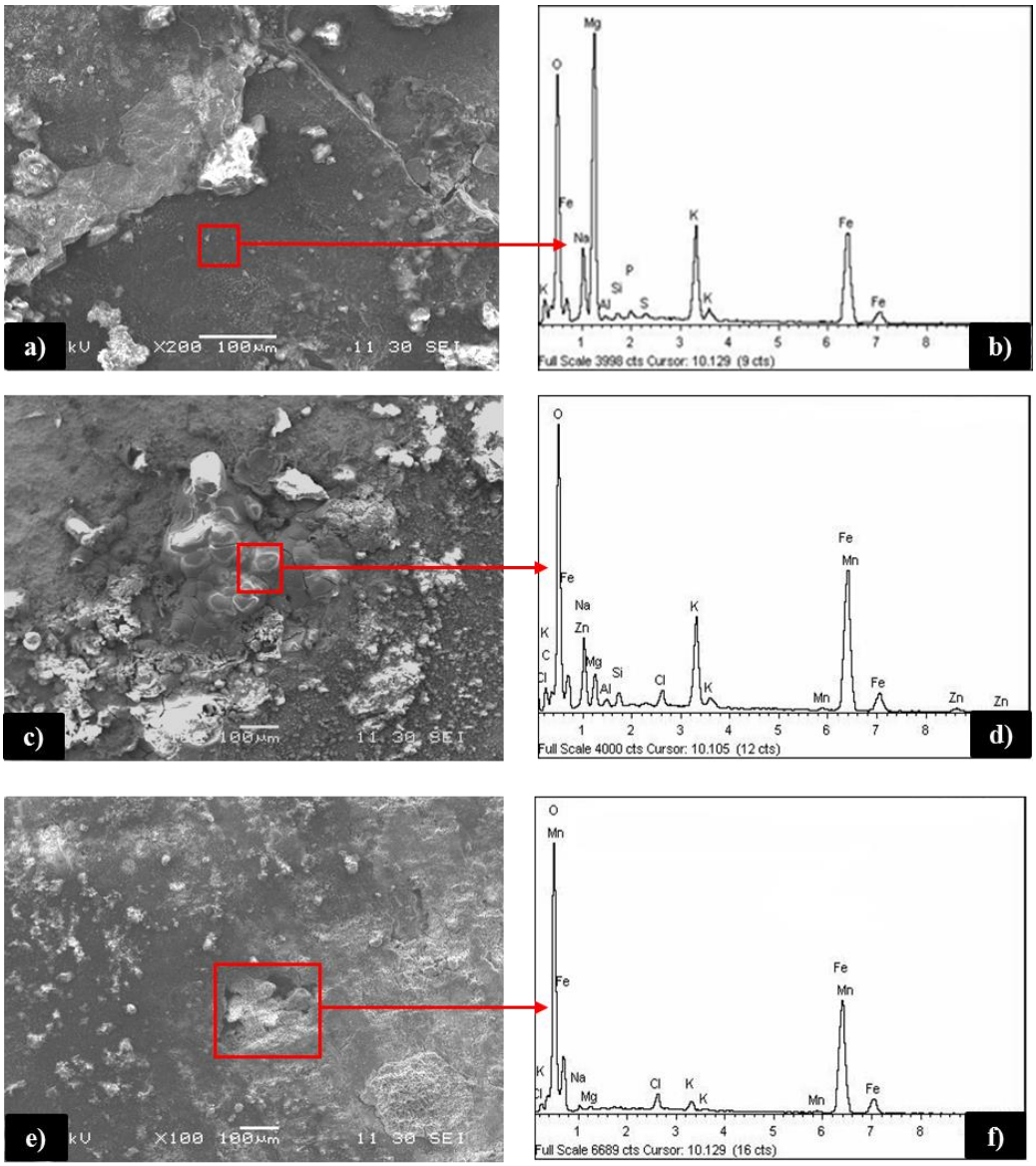


**Figure 5. UHT and LHT SEM micrographs and EDS spectra. (a) upper hot tank (UHT) section micrograph; (b) upper hot tank (UHT) section EDS spectrum; (c) upper hot tank (UHT) corrosion spot micrograph; (d) upper hot tank (UHT) corrosion spot EDS spectrum; (e) lower hot tank (LHT) section micrograph, (f) lower hot tank (LHT) corrosion spot EDS spectrum**

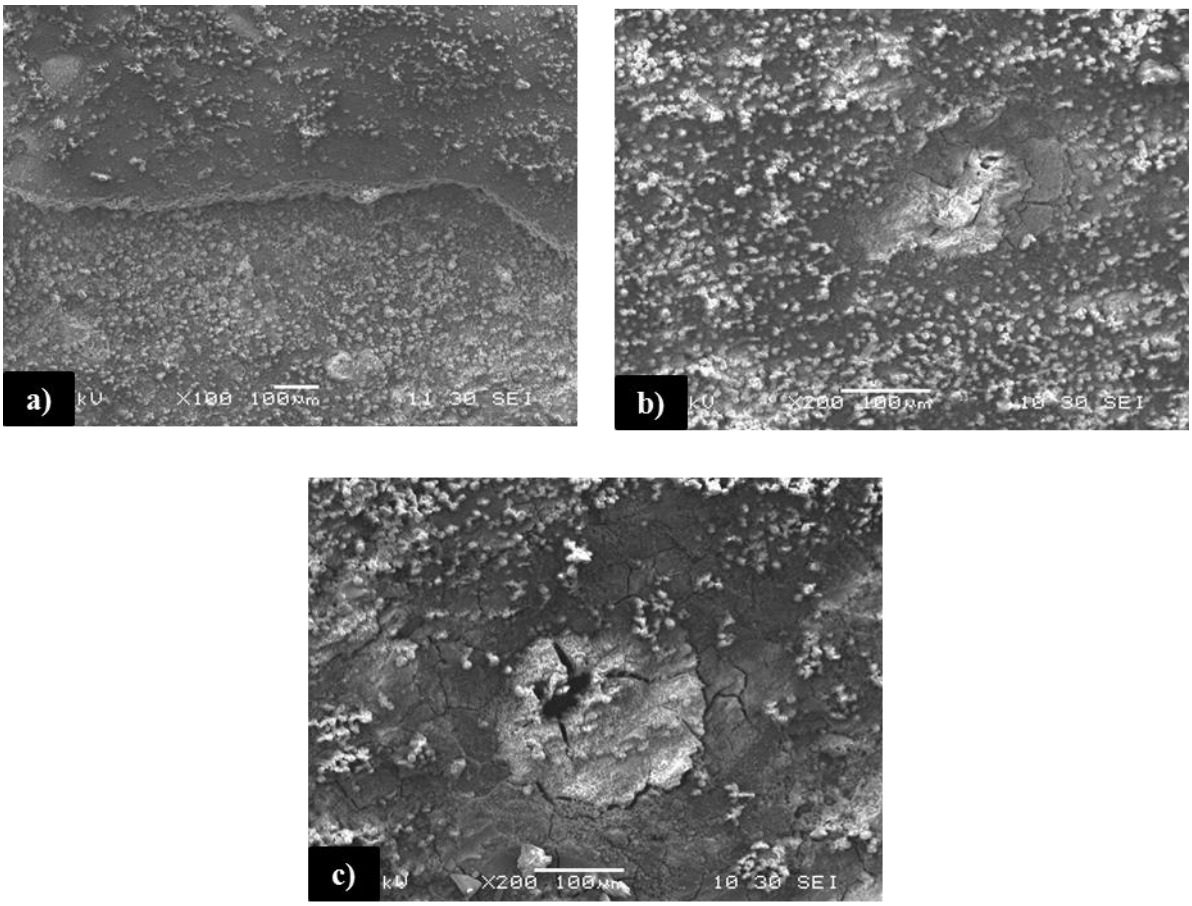


**Figure 6. UCT and LCT SEM micrographs and EDS spectra. (a) upper cold tank (UCT) section micrograph; (b) upper cold tank (UCT) corrosion spot micrograph; (c) lower cold tank (LCT) corrosion spot micrograph**

XRD analysis was carried out over the surface of tank plates. Periclase (MgO) was detected in the XRD spectra which is aligned with EDS analysis showed in Figure 5. As explained before, MgO is produced due to the decomposition of magnesium nitrate and is typically found in the surface of metal components exposed to solar salts [34]. Iron oxide in the form of magnetite ($Fe_{<}O_4$) was also detected in XRD spectra. This observation was also found by the authors in previous studies which evaluate the corrosion performance of carbon steel coupons immersed in the storage tanks of the pilot plant under discussion in this manuscript [31]. In addition to MgO and $Fe_3O_4$, other species such as $NaNO_3$, $KNO_3$, and iron was detected in the spectra. This chemistry was similar corrosion products generated in the molten salts pump sections under evaluation. Figure 7 shows XRD spectra for UHT (Figure 7a) and UCT (Figure 7b) as examples of the results obtained.

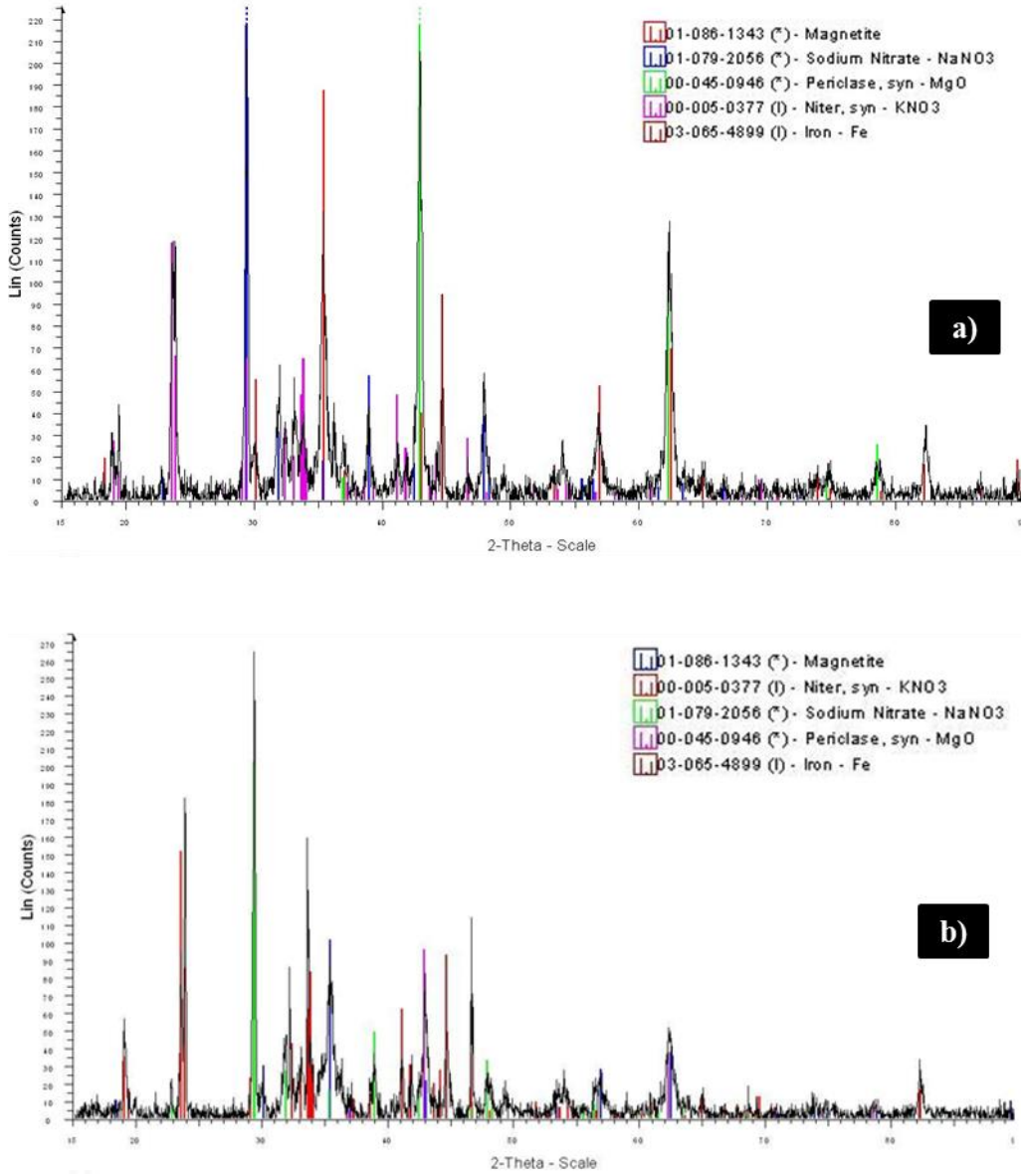


**Figure 7. XRD spectra. (a) Upper hot tank (UHT); (b) Upper cold tank (UCT)**

## Metallographic evaluation

Optical micrograph in Figure 8a showed the oxide scale delamination observed in certain areas on the UHT plate. The small localized corrosion areas (more reddish) detected in the SEM study are shown in Figure 8b. This latter figure shows the maximum penetration depth observed in the different embedded sections of the UHT plate. The corrosion progression through base metal was about 140 microns. Optical micrographs in Figure 8 also show the different morphology characteristics of the oxide layer on the LHT plate. LHT also shows small localized corrosion areas, which barely penetrated the material (Figure 8d). Oxide layer delamination was not observed on this sample. The corrosion morphology and extension on the UCT and LCT samples was practically identical to those observed on the LHT plate section. A partially detached and cracked oxide layer with constant thickness was observed in addition to micro-areas of localized corrosion (Figure 9a and Figure 9b).

Corrosion phenomena detected in UHT is typically called as breakaway corrosion being characterized by non-protective oxide scales. This type of corrosion may occur on carbon steels, generally at temperatures above 400 ºC, although in certain conditions, such as with the presence of $CO_2$, chlorides or water vapor on the medium, this phenomenon may happen at lower temperatures. Thus, in the presence of $CO_2$, the temperature from which this breakaway corrosion may be provoked is in the range of 350 ºC [35]. Steel parts under this phenomenon are exposed to higher corrosion rates due to the non-protective performance of corrosion products generated over the base metal. Conditions under which the preheating of the hot tank was carried out would be the origin of the non-protective oxides generation in areas intermittently exposed to nitrates salts. The main goal of tanks preheating was to adequate the metal temperature of the vessel avoiding both, metal thermal shocks during filling and molten salts freezing. Tanks preheating system was an 850 kW power preheated air blower with propane burner. In addition to metal temperature increasing prior to salts filling, preheating equipment was also used as a back-up heating system during the first weeks of operation due to the elevate heat losses higher than expected and inclement weather during the start-up. Preheating system specification did not limit the amount of $CO_2$ introduced inside the tanks so that carbon steel under intermittent exposure was exposed to the combination of chlorides (coming from molten salts), $CO_2$ (coming from preheating system), and water vapor (due to salts hygroscopicity). Taking into account the corrosion morphology experienced by UHT plates, it is seen that this mixture ($CO_2$+Cl+$H_2O$) was especially aggressive in the hot tank due to higher temperature in this vessel.

On the other hand, localized phenomena were developed by carbon steels under all tested conditions, hot and cold tank in addition to continuous and intermittent molten salts exposure as previously stated during the evaluation of the metal surface by SEM. This corrosion attack was not previously detected by the authors in other studies developed with corrosion racks submerged in TES-PS10 storage tanks nor laboratory tests analyzing the corrosion performance of high chloride content nitrates salts [29,31]. Within this study, EDS spectra detected the presence of chloride within the corrosion products being able to take an important role in combination with storage tanks corrosion atmosphere leading the corrosion mechanism produced in these specific areas. The main reason for this different corrosion performance in the tanks would be linked to the exposure time. while the pilot plant was in operation for 30000 hours, corrosion coupons submerged inside the tank were exposed between 1680 and 8712 hours. The higher exposure time in the tank plates produced the accumulation of chlorides in the localized corrosion areas creating an accelerated corrosion process in these points. Chlorides concentration increasing was confirmed by a semi-quantitative EDS analysis of the salt adhered to the plate (Table 3).

**Table 3. Semiquantitative EDS analysis for LCT**

| | Element | (wt.%) |
|---|---|---|
| EDS salt analysis for LCT | O | 52.09 |
| | N | 16.63 |
| | Na | 14.24 |
| | K | 10.58 |
| | Cl | 3.68 |
| | Mg | 2.32 |
| | P | 0.46 |
| | Total | 100 |

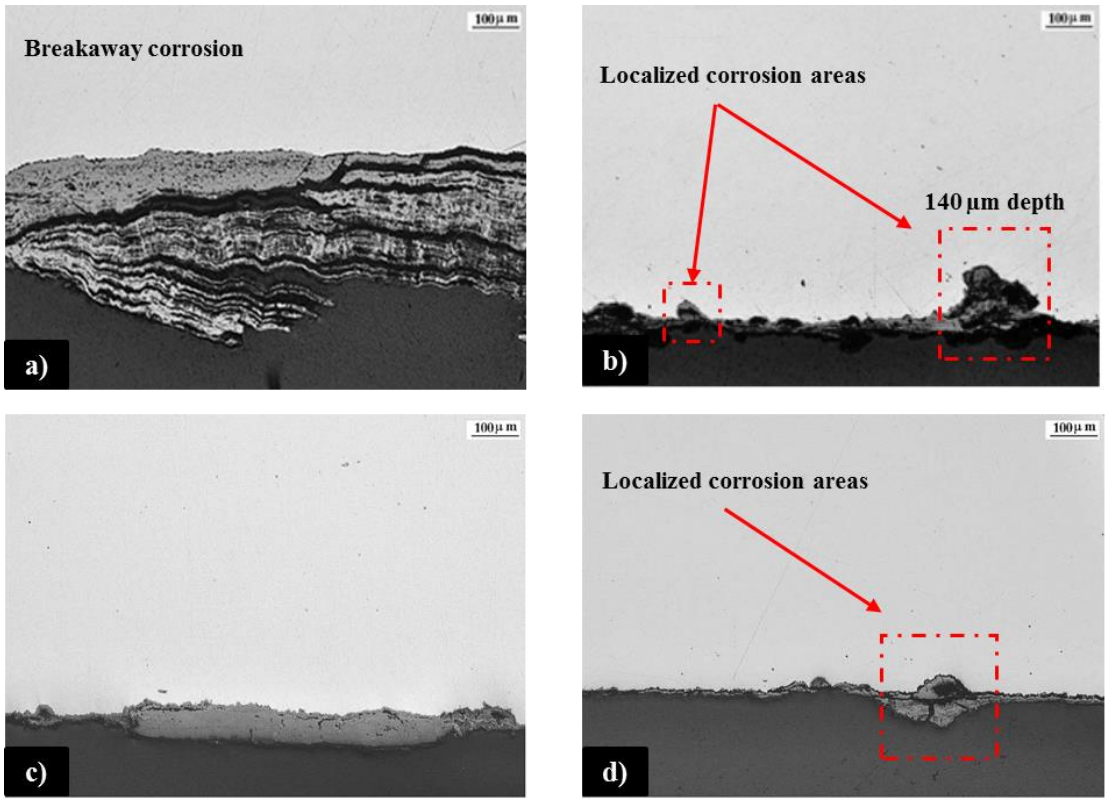


**Figure 8. Hot storage tanks shell sections micrograph. (a) Oxide scale delamination in upper hot tank (UHT) shell plate section; (b) Localized corrosion in upper hot tank (UHT) shell plate section; (c) Oxide scale in lower hot tank (LHT) shell plate section; (d) Localized corrosion in lower hot tank (LHT) shell plate section**

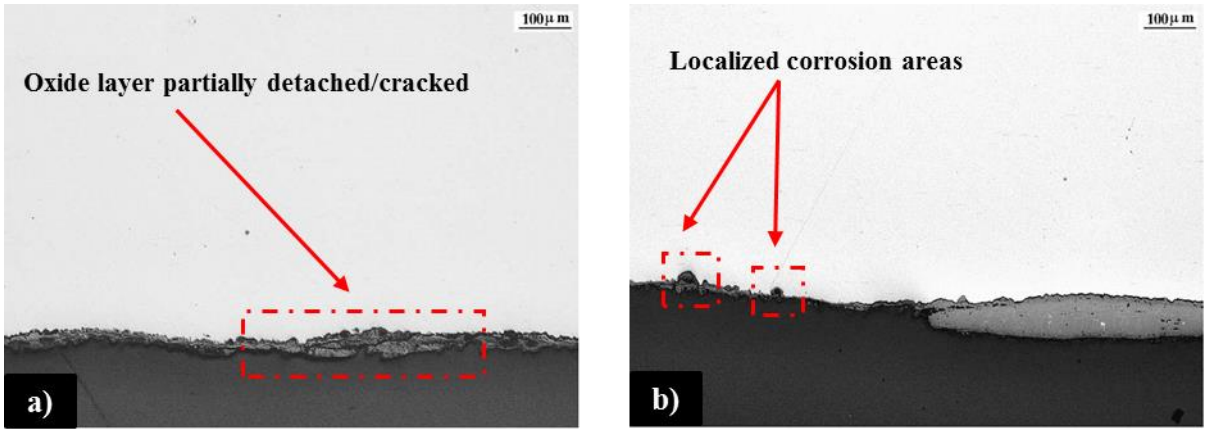


**Figure 9. Cold storage tanks shell sections micrograph. (a) Partially detached oxide layer in upper cold tank (UCT) shell plate section; (b) Localized corrosion in upper cold tank (UCT) shell plate section**

## Mechanical characterization

In addition to corrosion performance, mechanical properties of the carbon steel plates were tested after more than 30000 hours of operation. Accordingly, tensile tests were executed at room temperature and results obtained for yield strength, tensile strength and elongation are shown in

Table 4. In conclusion, yield strength, tensile strength, and elongation values were higher than the minimum ones required for A516 Gr70, in accordance with ASTM A516 standard.

**Table 4. Tensile test results for upper hot tank (UHT), lower hot tank (LHT), upper cold tank (UCT), and lower cold tank (LCT) sections**

| Component reference | Yield Strength (MPa) | Tensile Strength (MPa) | Elongation (%) |
|---|---|---|---|
| UHT Section | 384 | 521 | 34.0 |
| LHT Section | 379 | 519 | 35.0 |
| UCT Section | 371 | 512 | 32.5 |
| LCT Section | 369 | 515 | 33.5 |
| ASTM A516-10 Grade 70 | 260 (min.) | 485-620 | 21 (min.) |

## 3.2. Hot molten salts pump sections

**Visual inspection**

Figure 10a shows a photograph of the discharge pump pipe section (DP) after removal from the installation. The external and internal side of this component was continuously exposed to solar salts at an operating temperature in the range of 390 ºC. Salt residues were observed on the external surface as well as small areas of reddish-brown corrosion products. A longitudinal dry cut was made in the pipe section in order to examine the internal surface (Figure 10b). A uniform generalized corrosion was observed with a compact and firmly attached blackish oxide layer. In this sense, few small areas showed oxide layer detachment (Figure 10c). The pipe surface next to the flange weld showed small corrosion particles or aggregates, probably due to the corrosion of particles or contaminants generated during the welding of the pipe to the flange. Localized corrosion on this component was not detected (Figure 10d). On the other hand, Figures 11 shows different details of the discharge elbow (DE) section. The external surface kept most of the original paint, although there was evidence of salt residue and areas with slight generalized corrosion. The DE section was also cut for a detailed analysis of the internal surface (Figure 11a). In general, a compact adherent blackish oxide layer was present in most of the internal surface. However, some reddish corrosion spots on top of the initial blackish oxide layer could be observed (Figure 11). Several pores or cavities are detected on the internal surface (red rectangles in Figure 11b).

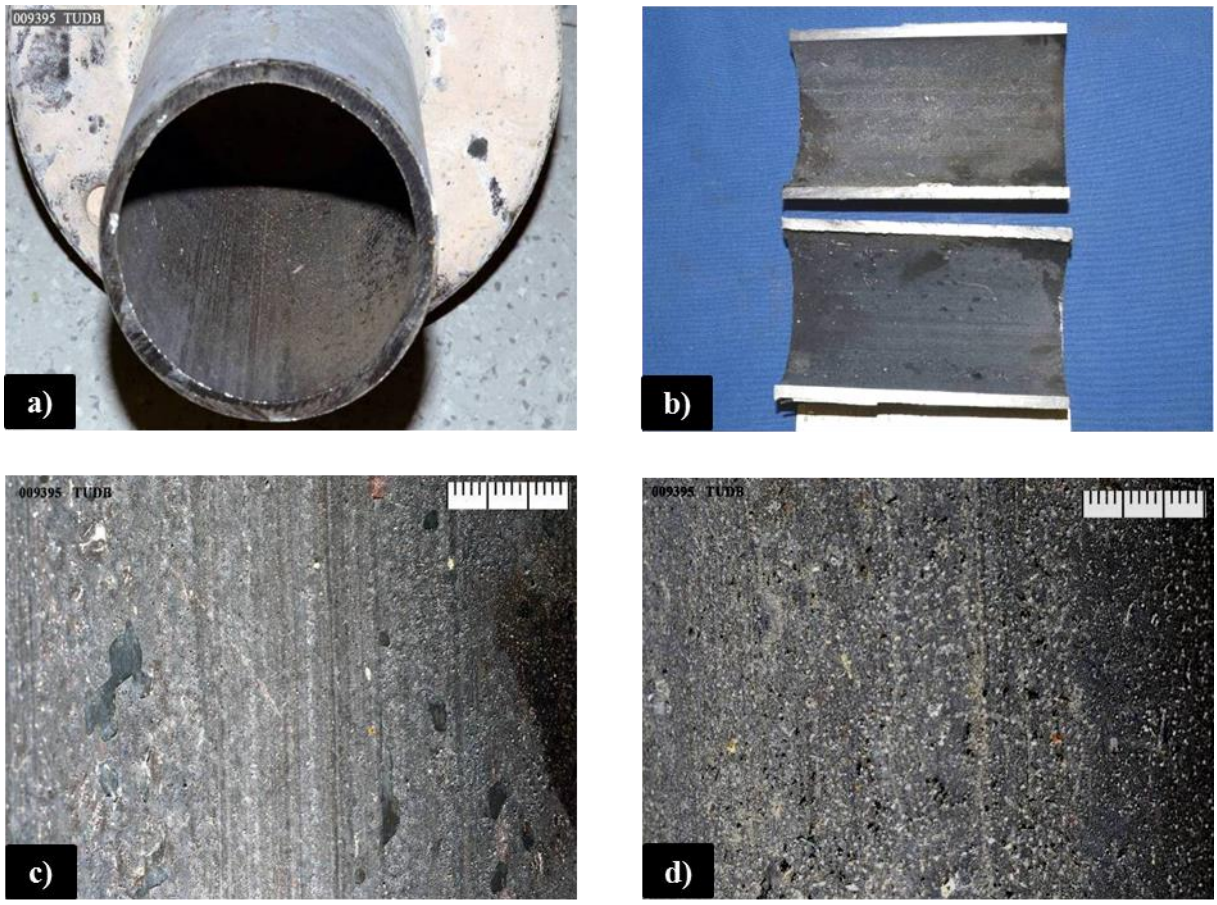


**Figure 10. Discharge pump (DP) sections visual inspection. (a) DP overall detail; (b) Dry cut over DP section; (c) DP internal section detail; (d) DP internal section detail in an area close to nozzle joint**

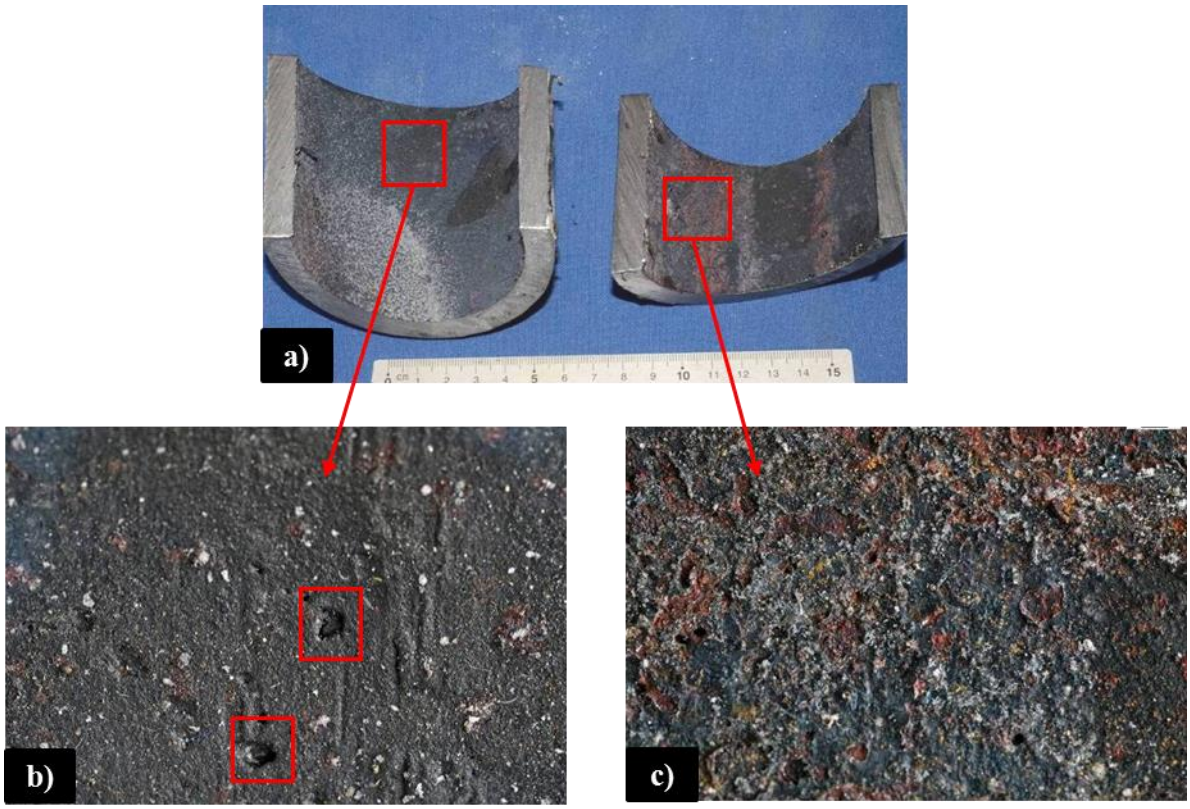


**Figure 11. Discharge elbow (DE) sections visual inspection. (a) Dry cut over DE section; (b) DE internal section highlighting cavities; (c) DE internal section highlighting reddish corrosion spots**

**Surface SEM/EDS analysis**

The internal surface of the pipe was examined by SEM-EDS for a detailed analysis of the corrosion products generated in the metal surface characterizing chemical elements involved in the oxides layers. The electron micrograph in Figure 12a shows a detail of the internal surface of the DP section. The oxide layer was partially detached in some areas. The EDS analysis of this layer indicated that it was basically comprised of Fe and O, as iron oxide, together with significant quantities of Na, K and Mg as constituents of the nitrate salts (Figure 12b). The DP external surface showed a similar morphology to that found on the internal surface. In this case, the original coating layer was cracked in several areas (Figure 13a). Beneath this cracked layer, the pipe surface looked rusted. The EDS analysis conducted on the painted surface detected a significant amount of the salt residue. The presence of calcium (Ca), copper (Cu), and aluminum (Al) on the coating would be associated to the paint itself (Figure 13c). The appearance of the internal surface of DE sample in a pore-free area is shown in Figure 14a. The electron micrograph showed a thin and compact oxide layer over the base metal. The micrograph in Figure 14c showed the aspect of the micropores observed on the internal surface of the component in Figure 11b. Finally, EDS spectra were in agreement with previous profiles analyzed within this study in previous components (Figure 14b and Figure 14d).

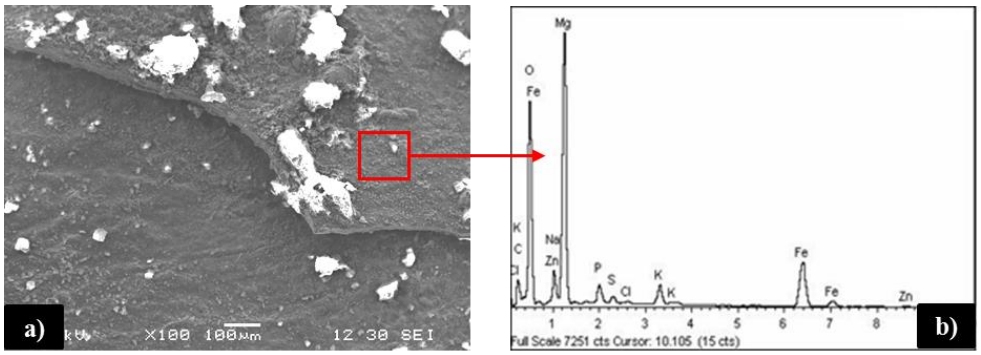


**Figure 12. Discharge pump (DP) internal surface micrograph and EDS spectrum. (a) DP internal surface SEM; (b) DP internal section EDS spectrum**

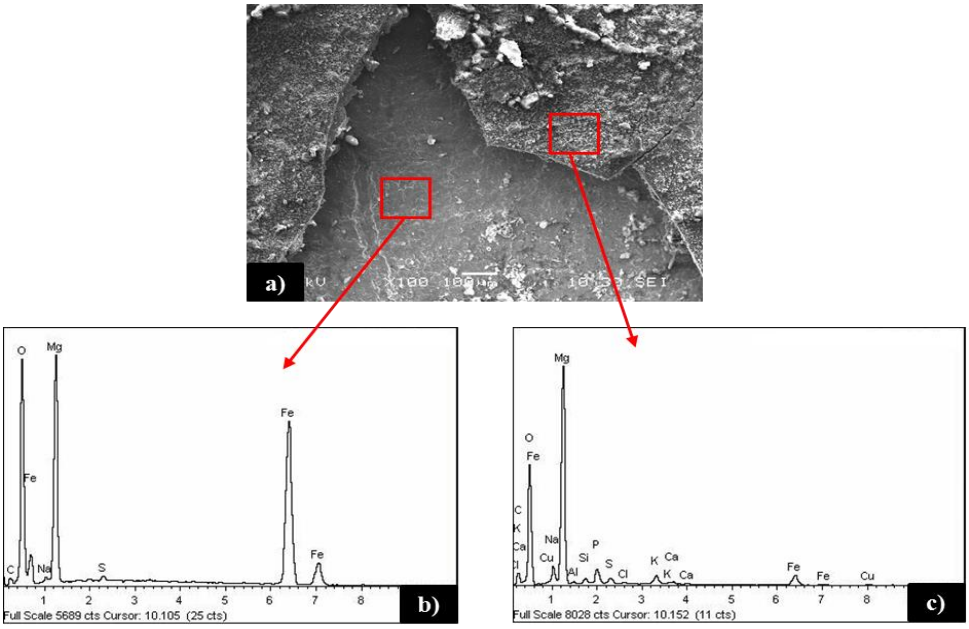


**Figure 13. Discharge pump (DP) external surface micrograph and EDS spectra. (a) DP external surface SEM; (b) DP external surface EDS spectrum (below coating); and (c) DP external surface EDS spectrum (coating)**

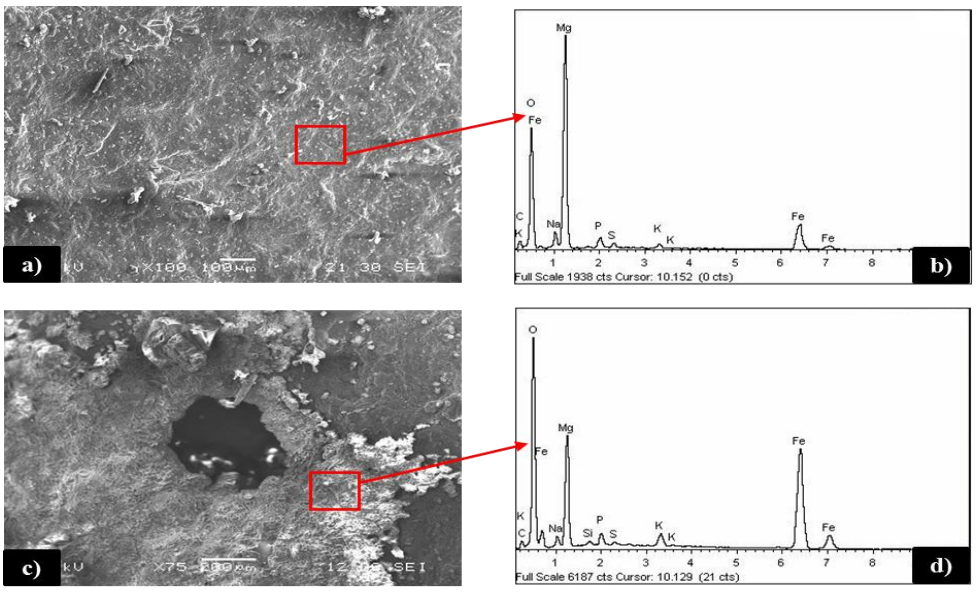

**Figure 14. Discharge elbow (DE) internal surface micrograph and EDS spectra. (a) DE free-cavities area SEM; (b) DE free-cavities area EDS spectrum; (c) DE cavity SEM; (d) DE cavity EDS spectrum**

## Metallographic evaluation

Metallographic specimens were prepared from transversal sections extracted from the DP sample under evaluation to be analyzed by using optical microscopy. The internal surface of DP section had an almost uniform and firmly attached oxide layer (Figure 15a). The external surface showed a similar corrosion to that observed on the internal one. In this way, corrosion products were similar in thickness and shape in zones where coating was practically removed (Figure 15c). DP sample showed a ferrite-perlite microstructure which is typical of in carbon steels (Figure 15b and Figure 15d). Transversal sections were also cut from DE sample for microstructural analysis. Then, Figure 16a shows the internal surface detecting a very well adhered and thin oxide layer. Micro-pores discussed in previous sections are shown in Figure 16b and Figure 16c being mostly located on the internal surface of the elbow. The size of these cavities was variable, being able to reach up to 1 mm in size. Accordingly, the metallurgical quality of the cast steel was not the most suitable because of many pores were observed in the original material.

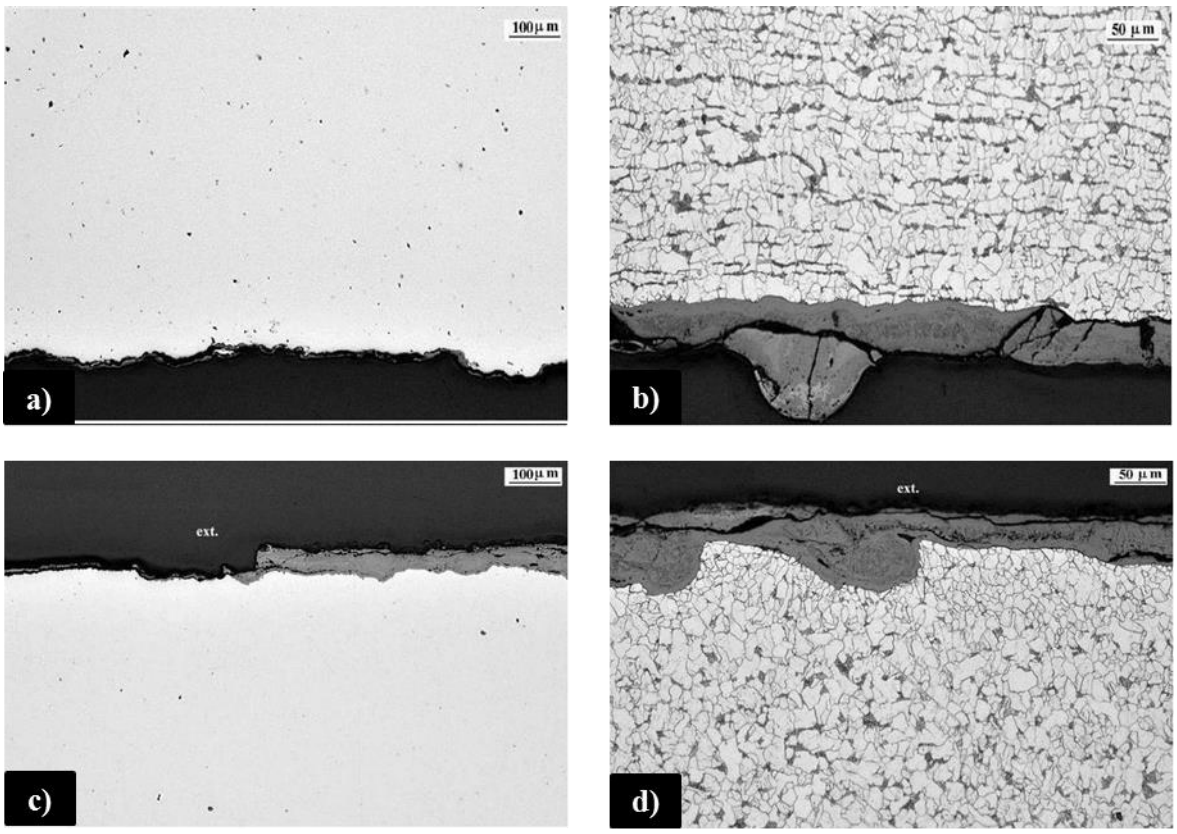


**Figure 15. Discharge pump (DP) sections evaluation. (a) DP internal surface; (b) DP internal surface microstructure with metallographic etching; (c) DP external surface; (d) DP external surface microstructure with metallographic etching**

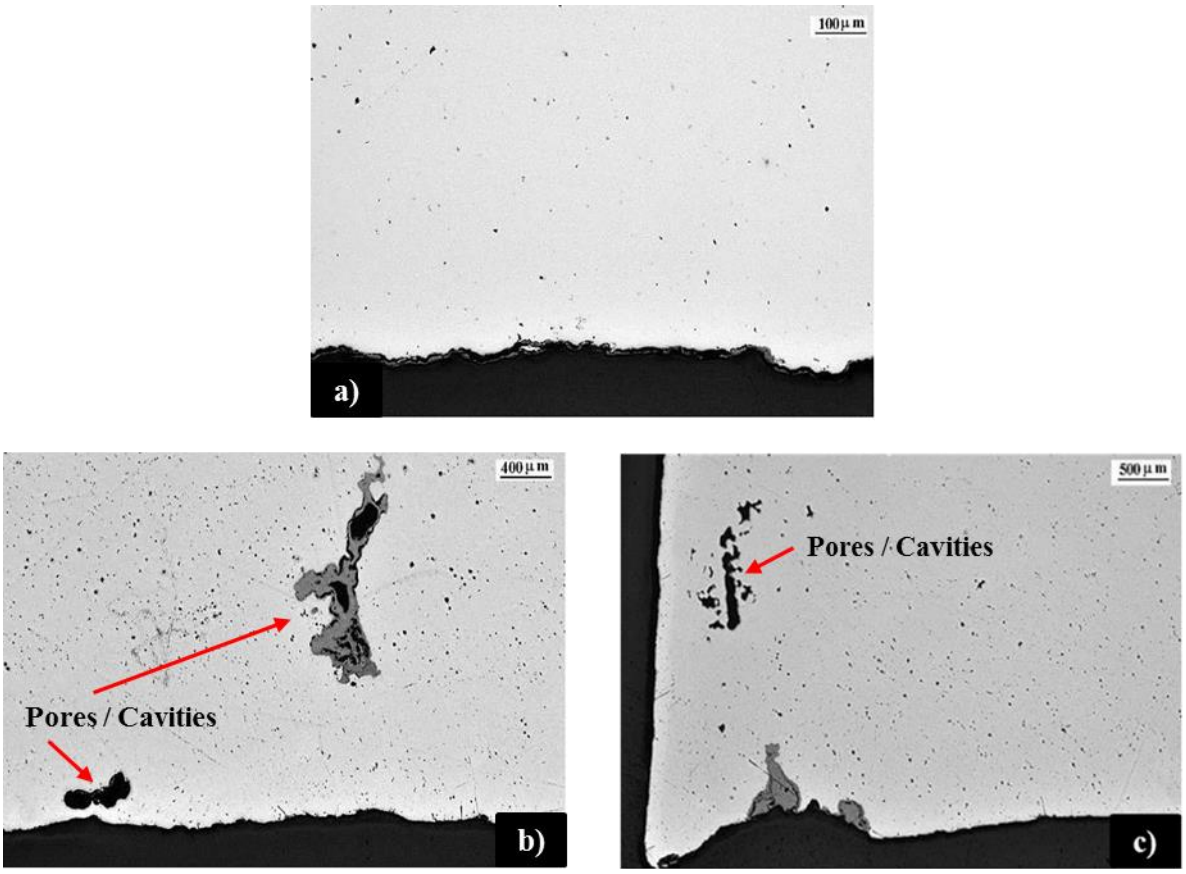


**Figure 16. Discharge elbow (DE) section evaluation. (a) DE internal surface; (b) and (c) DE internal surface highlighting cavities**

## 4. Conclusions

This study analyzes the corrosion performance of sections extracted from storage tanks and hot molten salts pump removed from TES-PS10 pilot plant after almost four years of continuous operation being exposed to high temperature solar salts. Results within this postmortem analysis are highly interesting for this field of knowledge because the operation conditions to which alloys under study were subjected are very similar to those of a commercial facility, which are difficult to reproduce in the lab. The main conclusions extracted from this paper to take into account in the design of commercial TES systems in terms of corrosion are as follow:

- UHT sample showed areas on the internal surface characterized by the growth of an exfoliating/delaminating non-protective oxide scale caused by breakaway corrosion phenomenon. The reason why this attack occurred in the hot storage tank plates exposed to intermittent exposure was due to the combination of $CO_2$, water vapor and chlorides at high temperature. This mixture was in contact with carbon steel during the preheating of the vessel and later in the first weeks of operation when the preheating equipment was used as a back-up heating system. Because of this result, the design of commercial preheating systems must assure that a minimum amount of $CO_2$ is introduced during the preheating process to avoid the breakaway corrosion phenomenon.

- LHT, UCT and LCT samples presented uniform corrosion developing well adhered and protective oxides layers consisting in iron oxides as expected taking into account previous studies carried out by the authors [31].

- All tanks plates under evaluation developed small areas of localized corrosion barely penetrate through base metal. EDS spectra showed the presence of Cl in these corrosion nodules. Chlorides are expected to have an important role promoting the formation of this localized corrosion spots. Then, solar salts specification to be used in commercial projects must minimize the amount of chlorides avoiding two main drawbacks: (i) high corrosion rates as corrosiveness of nitrates salts is intimately related to chlorides percentage [29], and (ii) localized attack through base metal as analyzed in this study.

- Mechanical strength for all tanks plates was in agreement with ASTM A516 standard. In this way, yield strength, tensile strength and elongation values were above the minimum required by the standard.

- Both hot pump sections, DP and DE, showed uniform corrosion. Accordingly, a compact, adherent and quite uniform oxide layer was observed for both samples. Moreover, corrosion-erosion phenomena due to molten salts flowing through the discharge elbow or discharge pipe were not detected.

- Metallurgical quality of the cast steel was deficient detecting many pores/cavities in the original material. The possible coalescence of these cavities could lead to an unexpected failure of the component for long-term expositions. An exhaustive quality control over sections manufactured by casting processes must be carried out to avoid in service failures.

- Significant quantities of Na, K, and Mg coming from nitrate salts were detected by EDS analysis for all components under evaluation. The stichometry of the corrosion products was identified by XRD spectra detecting magnetite ($Fe_3O_4$) and periclase (MgO).

- There are differences between corrosion damage displayed by carbon steel tank plates within this study and previous tests carried out using corrosion coupons submerged inside the storage tanks of TES-PS10 pilot plant [31].

  Breakaway corrosion detected in UHT plate was not observed in the corrosion coupons. Corrosion coupons were affected by preheating gases only during tank preheating due to these coupons were completely submerged in molten salts after filling. On the other hand, UHT tank plate was exposed to this atmosphere during the preheating and after the salts filling due to the preheating equipment was used as a back-up heating system during the first weeks of operation to compensate heat loss. The combined effect of high exposure time to $CO_2$ and high temperature in the hot tank produced the breakaway corrosion displayed by UHT plates [35].

  Localized corrosion nodules were detected for all plates under evaluation (hot and cold tank for continuous and intermittent exposition to molten salts). On the contrary this corrosion damage did not occur in the corrosion coupons. The higher exposition time for tank plates (30000 hours vs. 8712 hours) produced a local chloride concentration increasing generating these corrosion nodules in the material. Chlorides increase molten salts aggressiveness over carbons steels and low alloyed steels due to the formation of chlorine ($Cl_2$) [36]. Corrosion mechanism is as follows; once chlorine has been produced by de combination of chlorides ions, diffusion processes through oxides layer are

produced. Chlorine react with the steel alloying elements to form metal chlorides at the steel/oxides layer interface. Metal chlorides vapor pressure is relatively high at the interface and the evaporation of these species is produced. Then, metal chlorides diffuse back through the alloy oxides layers of the steel. Finally, metal chlorides are oxidized to metal oxides as magnetite and hematite. Then, chlorine is again produced being this specie available to start the process described previously.

$$Fe + Cl_2 \rightarrow FeCl_2(s) \tag{11}$$

$$FeCl_2(s) \rightarrow FeCl_2(g) \tag{12}$$

$$3FeCl_2 + 2O_2 \rightarrow Fe_3O_4 + 3Cl_2 \tag{13}$$

$$2FeCl_2 + \frac{3}{2}O_2 \rightarrow Fe_2O_3 + 2Cl_2 \tag{14}$$

- Despite the localized corrosion phenomena and breakaway corrosion previously discussed, the corrosion damage extension over all components tested in this paper was under the design basis of the installation.

Summarizing, the corrosion phenomena suffered by components under evaluation could be corrected by applying lessons learned previously discussed. Accordingly, breakaway corrosion (250 microns corrosion damage extension) will be avoided minimizing the amount of $CO_2$ during the tanks preheating. On the other hand, localized corrosion (140 microns corrosion damage extension) will be avoided/minimized using high quality salt mixtures with low amount of chlorides such as refined or synthetic grades. Current corrosion allowances specified for commercial storage systems would cover the corrosion damage extensions measured within this manuscript for the lifetime of the plant. Moreover, applying lessons learned previously explained will minimize the expected corrosion rates resulting in a more conservative design.

As conclusion, the materials selection analyzed within this postmortem evaluation is valid from corrosion point of view to be used in the design of commercial TES system using solar salts as storage fluid at temperatures in the range 290-390 ºC.

**Acknowledgements**

The research leading to these results has received funding from Spanish government (Fondo tecnológico IDI-20090393, ConSOLida CENIT 2008-1005). The work is partially funded by the Spanish government (ENE2011-28269-C03-02, ENE2011-22722, ENE2015-64117-C5-1-R, and ENE2015-64117-C5-2-R). The authors would like to thank the Catalan Government for the quality accreditation given to their research group GREiA (2017 SGR 1537) and research group DIOPMA (2017 SGR 138). GREiA and DIOPMA are certified agents TECNIO in the category of technology developers from the Government of Catalonia.

## References


[1] Siva V, Kaushik S, Ranjan K, Tyagic S. State-of-the-art of solar thermal power plants: A review. Renewable and Sustainable Energy Reviews, 2013; 27: 258-273

[2] Zhanga H, Baeyens J, Degréve J. Concentrated solar power plants: Review and design methodology. Renewable and Sustainable Energy Reviews, 2013; 22: 466-481

[3] Jebasingh VK, Herbert GM. A review of solar parabolic trough collector. Renewable and Sustainable Energy Reviews, 2016; 54: 1085-1091

[4] Behar O, Khellaf A, Mohammedi K. A review of studies on central receiver solar thermal power plants. Renewable and Sustainable Energy Reviews, 2013; 23: 12-39

[5] Abbas R, Muñoz-Antón J, Valdés M, Martínez-Val JM. High concentration linear Fresnel refectors. Energy Conversion and Management, 2013; 72: 60-68.

[6] Kongtragool B, Wongwises S. A review of solar-powered Stirling engines and low temperature differential Stirling engines. Renewable and Sustainable Energy Reviews, 2003, 7: 131-154

[7] Liu M, Steven NH, Bell S, Belusko M, Jacob R, Will G, Saman W, Bruno F. Review on concentrating solar power plants and new developments in high temperature thermal energy storage technologies. Renewable and Sustainable Energy Reviews, 2016; 53: 1411-1432

[8] Cabeza L, Galindo E, Prieto C, Barreneche C, Fernández AI.. Key performance indicators in thermal energy storage: Survey and assessment. Renewable Energy, 2015; 83: 820-827

[9] Gil A, Medrano M, Martorell I, Lázaro A, Dolado P, Zalba B, Cabeza L. State of the art on high temperature thermal energy storage for power generation. Part 1 - Concepts, materials and modelization. Renewable and Sustainable Energy Reviews, 2010; 14: 31-55

[10] González-Roubaud E, Pérez-Osorio D, Prieto C. Review of commercial thermal energy storage in concentrated solar power plants: Steam vs. molten salts. Renewable and Sustainable Energy Reviews, 2017; 80: 133-148

[11] Sena-Henderson L. Advantages of using molten salts, SANDIA National Laboratories, 2006.

[12] Herrmann U, Kelly B, Price H. Two-tank molten salt storage for parabolic trough solar power plants. Energy, 2004; 29: 883-893

[13] Kearney D, Kelly B, Herrmann U, Cable R., Pacheco J, Mahoneye R, Price H, Blake D, Navac P, Potrovitza N. Engineering aspects of a molten salt heat transfer fluid in a trough solar field. Energy, 2004; 29: 861-870

[16] Horsman P, Conway B. Yeager E. Comprehensive Treatise of Electrochemistry, Vol 7, Plenum Press, 1983

[17] Lay G. High Temperature Corrosion and Materials Applications, ASM International, 2007

[18] De Jong J, Broers G. Electrochemistry of the oxygen electrode in the KNO3-KO2 system, a comparative study. Electrochimica Acta, 1977; 22: 565-571

[19] Singh I, Sultan S, Balakrishnan K. Cyclic voltammetric behaviour of platinum in dried and wet nitrates melt. Electrochimica Acta, 1993; 38: 2611-2615

[20] El Hosary AA, Shams El Din AM. A chronopotentiometric study of the stability of oxide ion in molten nitrates. Electrochimica Acta, 1971; 16: 143-149

[21] Kruizenga AM, Gill DD, LaFord M, McConohy G. Corrosion of High Temperature Alloys in Solar Salt at 400, 500, and 680°C (SAND 2013-8256). Sandia National Laboratories, 2013

[22] Kruizenga AM, Gill DD, LaFord M. Materials Corrosion of High Temperature Alloys Immersed in 600°C Binary Nitrate Salt (SAND 2013-2526). Sandia National Laboratories, 2013

[23] Goods S., Bradshaw R., Prairie M. Chavez J. Corrosion of stainless steels and carbon steels in molten mixtures of industrial nitrates (SAND 94-8211), SANDIA National laboratories, 1994

[24] Bradshaw R. Oxidation and Chromium Depletion of Alloy 800 and 316SS and by Molten NaNO3 - KNO3 at Temperatures above 600°C (SAND86-9009), SANDIA National Laboratories, 1987

[25] Bradshaw R, Goods S. Corrosion Resistance of Stainless Steels during Thermal Cycling in Alkali Nitrate Molten Salts (SAND2001-8518), SANDIA National Laboratories, 2001

[26] Fernández AG, Lasanta MI, Pérez FJ. Molten Salt Corrosion of Stainless Steels and Low-Cr Steel in CSP Plants. Oxidation of metals, 2012; 78: 329:348

[27] Walczak M, Pineda F, Fernández AG, Mata-Torres C, Escobar RA. Materials corrosion for thermal energy storage systems in concentrated solar power plants. Renewable and Sustainable Energy Reviews, 2018; 86: 22-44

[28] Bradshaw RW, Clift WM. Effect of chloride content of molten nitrate salt on corrosion of A516 carbon steel (SAND 2010-7594), SANDIA National laboratories, 2010

[29] Ruiz-Cabañas FJ, Prieto C, Madina V, Fernández AI, Cabeza LF. Materials selection for thermal energy storage systems in parabolic trough collector solar facilities using high chloride content nitrate salts. Solar Energy Materials and Solar Cells, 2017; 163: 134-147

[30] Prieto C, Gallardo-González J, Ruiz-Cabañas FJ, Barreneche C, Martínez M, Segarra M, Fernádez AI. Study of corrosion by Dynamic Gravimetric Analysis (DGA) methodology. Influence of chloride content in solar salt. Solar Energy Materials and Solar Cells, 2016; 157: 526:532

[31] Ruiz-Cabañas FJ, Prieto C, Osuna R, Madina V, Fernández AI, Cabeza LF. Corrosion testing device for in-situ corrosion characterization in operational molten salts storage tanks: A516 Gr70 carbon steel performance under molten salts exposure. Solar Energy Materials and Solar Cells, 2016; 157: 383-392

[32] Prieto C, Osuna R, Fernández AI, Cabeza LF. Thermal storage in a MW scale. Molten salt solar thermal pilot facility: Plant description and commissioning experiences. Renewable Energy, 2016; 99: 852-866

[33] Prieto C, Osuna R, Fernández AI, Cabeza LF. Molten salt facilities, lessons learnt at pilot plant scale to guarantee commercial plants; heat losses evaluation and correction. Renewable Energy, 2016; 94: 175-185

[34] Prieto C, Ruiz-Cabañas FJ, Rodríguez-Sánchez A, Rubio C, Fernández AI, Martínez M, Oró E, Cabeza LF. Effect of the impurity magnesium nitrate in the thermal decomposition of the solar salt. Solar Energy, 2018

[35] German PA, Hill AC, Taylor MR. Mild steel oxidation in $CO_2$-cooled reactors. Gas Cooled Reactors Today. Proceedings of the conference, Bristol, 20-24, 1982

[36] Grabke HJ, Reese E, Spiegel M, The effects of chlorides, hydrogen chloride, and sulfur dioxide in the oxidation of steels below deposits, Corrosion Science, 1995; 37: 1023-1043